Hindawi Publishing Corporation
Journal of Nanomaterials
Volume 2015, Article ID 412071, 8 pages
http://dx.doi.org/10.1155/2015/412071

Research Article

Preparation and Characterization of Highly Flexible $Al_2O_3/Al/Al_2O_3$ Hybrid Composite

Zhijiang Wang,[1] Henry Hu,[2] and Xueyuan Nie[2]

[1]*School of Chemical Engineering and Technology, Harbin Institute of Technology, Harbin 150001, China*
[2]*Department of Mechanical, Automotive and Materials Engineering, University of Windsor, Windsor, ON, Canada N9B 3P4*

Correspondence should be addressed to Henry Hu; huh@uwindsor.ca and Xueyuan Nie; xnie@uwindsor.ca

Received 22 October 2015; Accepted 15 December 2015

Academic Editor: Zhengping Zhou

The natural brittleness of oxide ceramics heavily inhibits their more extensive applications. In present research, a highly flexible $Al_2O_3/Al/Al_2O_3$ hybrid composite was fabricated by employing plasma electrolysis oxidation to *in situ* grow alumina layers on Al foil, in which an outside layer of nanostructured polycrystalline oxide ceramic was composed of nanosized grains with the size of around 17 nm. Due to shear band formation, nanosized circle bubbles prolonging the crack path, grain rotation, and deformation, the fabricated $Al_2O_3/Al/Al_2O_3$ hybrid composite contains no observable cracks even after being bent on a cylindrical bar with a curvature of 1.5 mm. The composite exhibits alumina stiffness at the elastic stage and aluminum ductility during plastic deformation, which provides high flexibility with the well-integrated properties of the components. In a synergistic interaction, the alumina on the outside exhibited a strain of 0.33% at room temperature, which was higher than optimum value of 0.25% presented by reported most flexible oxide ceramics. With the unique characteristics and properties, the $Al_2O_3/Al/Al_2O_3$ composite demonstrates a great potential for various engineering applications.

1. Introduction

The excellent properties of oxide ceramics, such as chemical and thermal stability, high strength, and wear resistance, make it attractive for engineering applications [1, 2]. However, the natural brittleness of oxide ceramics becomes a main obstacle for their more extensive applications. Researchers have been devoted to find flexible oxide ceramics. Although certain types of superplastic ceramics and glass ceramics can be flexible at an elevated temperature, room-temperature flexibility similar to that exhibited by plastics or metals is not achieved for ceramics yet [3, 4].

Many natural materials like bone, tooth, and nacre, consisting of ceramic building blocks and organic biopolymer, have sophisticated structures with complex hierarchical designs of which properties exceed what could be expected from a simple mixture of their components. Inspired by such materials, some man-made hybrid composites with exceptional fracture resistance and structural capabilities have been developed by combining brittle minerals and ductile organic materials [5–8].

In the present research, highly flexible $Al_2O_3/Al/Al_2O_3$ hybrid composites, composed of brittle ceramic/ductile metal, were fabricated by plasma electrolytic oxidation (PEO) technique with polycrystalline alumina with a layer of nanosized grains growing *in situ* on Al foil. Although other methods, like chemical vapour deposition, physical vapour deposition, and welding technology, were developed to prepare Al_2O_3/Al hybrid composite [9], the flexibility of these kinds of materials had been seldom studied. The microstructural analyses indicate that the prepared $Al_2O_3/Al/Al_2O_3$ hybrid composite by PEO possessed a hierarchical structure. In macrostate, the sandwich material was composed of Al layer, inner alumina layer, and outer columnar alumina layer. The alumina consisted of α-Al_2O_3 and γ-Al_2O_3 phase with the average grain size of around 17 nm as well as amorphous phase. The results of mechanical testing reveal that the hierarchical structure of the $Al_2O_3/Al/Al_2O_3$ hybrid composites provides excellent tensile property and flexibility.

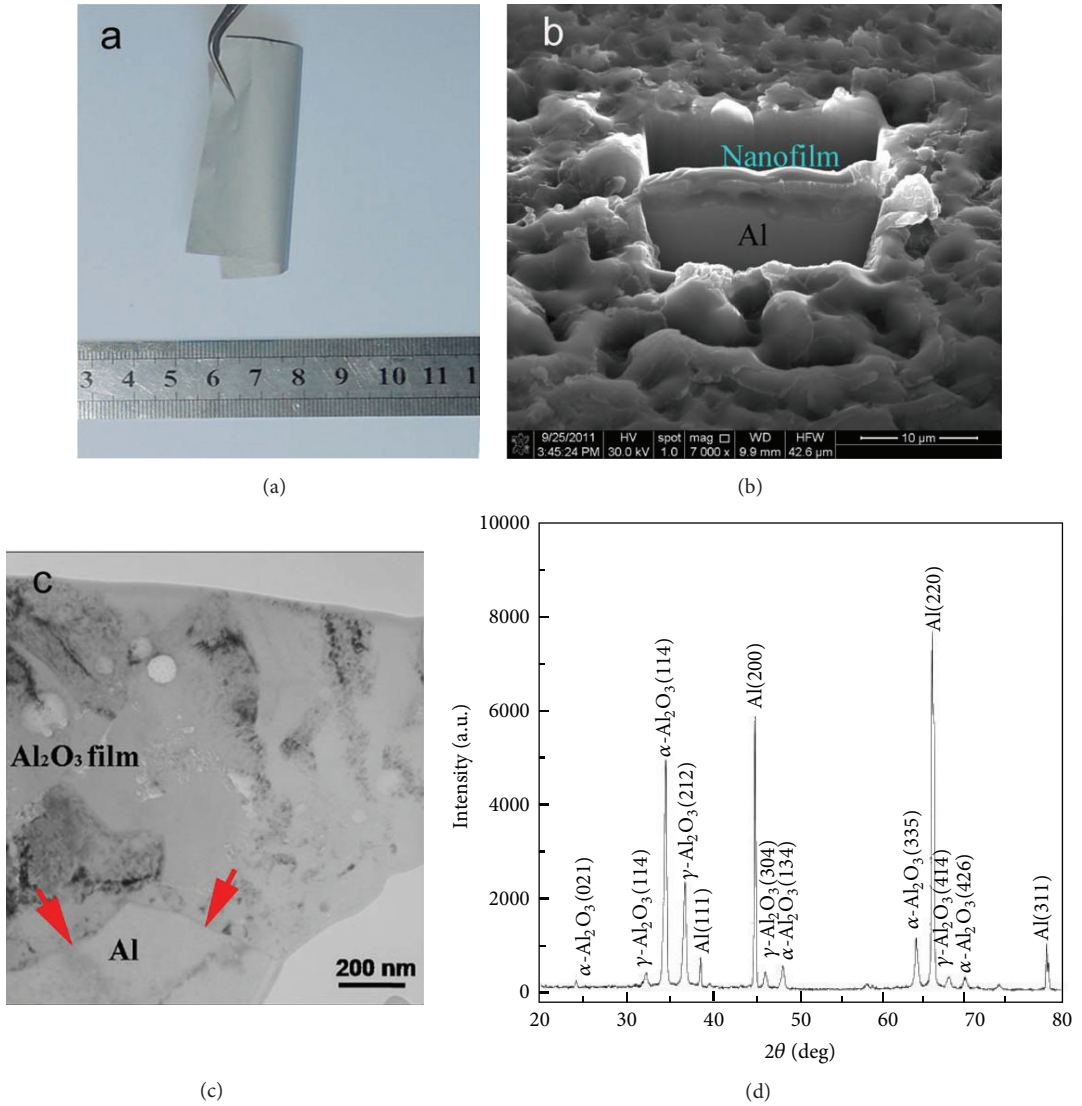

Figure 1: (a) Digital photograph, (b) cross section SEM image, (c) TEM image, and (d) XRD pattern of the sample. The cross section SEM image was taken at the state that the sample was covered with a Pt layer on the top and tilted 52° towards the ion beam. The red arrows in (c) point out the boundary of Al/Al_2O_3 film.

2. Experimental Section

The $Al_2O_3/Al/Al_2O_3$ hybrid composites were prepared by employing the PEO process, of which details were provided in [10]. As-received commercial 1100 Al foil (as the anode) and a stainless steel electrode (as the cathode) were connected to a power resource. The current regime was a unipolar pulsed DC supply under a current density of 0.04 A/cm^2. 4 g/L $NaAlO_2$ dissolved in deionized water was used as an electrolytic solution. The processing time was set as 4, 8, and 14 min. A cooling system maintained the electrolyte temperature below 30°C during the process.

A JOEL 2010 Scanning Electron Microscope (SEM) at a 15 kV operating voltage was employed to observe the sample surface morphologies, cross sections, and tensile fractographs. The phases of the coating were investigated using a Siemens D5000 X-ray diffractometer (Cu Kα radiation) with a scan range of 10°–90°. The nanocrystalline alumina film was examined using a transmission electron microscopy (TEM) at 120 KeV acceleration voltage (Philips CM12).

Static mechanical uniaxial in-plane tensile tests were conducted with a Zwick/Roell materials testing machine. Testing speed is set as 2.5 mm/min. The tensile properties, including yield strength (YS), ultimate tensile strength (UTS), and elongation to failure (Ef), were obtained based on the average of three tests to obtain mean value and corresponding error. After tensile test, the fracture and surface morphology of the coatings on the composite were observed by SEM.

3. Results and Discussion

3.1. Microstructure of the Al/Al_2O_3 Composite Sheet. Figure 1 shows the macro-morphology, cross section SEM and TEM images, and XRD pattern of the prepared $Al_2O_3/Al/Al_2O_3$

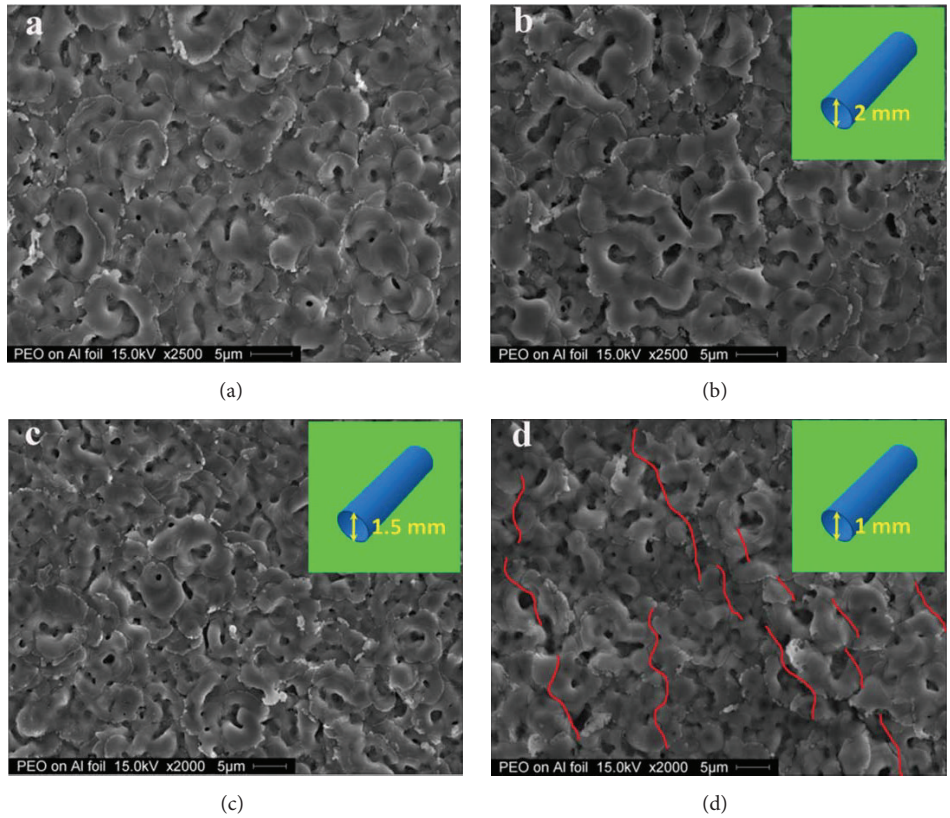

FIGURE 2: Bending experiments for the Al_2O_3 hybrid nanofilm (a) without bending and bending on a cylinder with a diameter of (b) 2 mm, (c) 1.5 mm, and (d) 1 mm, respectively. The cracks are noted by red curves.

hybrid composites under the PEO processing time of 8 min. From Figure 1(a), it can be found that the aluminum foil was covered with gray ceramic coating layers on both sides. The metal/ceramic composite sheet was highly flexible. It could be rolled into a circle, but without the presence of ceramic peeling off from the aluminum substrate. The cross section SEM image shows that the sandwich-like $Al_2O_3/Al/Al_2O_3$ composite sheet had a coating of alumina ceramic with a thickness of around 4.5 μm. Despite the fact that the shape of the interface between the Al substrate and alumina layer was irregular and wavy, there was no evident discontinuity at the interface of the coating/substrate, which implies the formation of a good bonding between them [10]. TEM image (Figure 1(c)) reveals that the crystalline size of the PEO film is about 17 nm. Meanwhile, microsized circle bubbles were randomly distributed in the film. This should result from the fact that, during the PEO process, oxygen and hydrogen gases were produced due to the electrolysis of water under a high voltage. The gases had a high tendency to be entrapped in the film during its growth. XRD pattern shown in Figure 1(b) indicates that the components of the ceramic film were α-Al_2O_3 and γ-Al_2O_3. The mean crystallite sizes of α-Al_2O_3 and γ-Al_2O_3 within the simple calculated using Scherrer's formula [11, 12] were 16.8 nm and 17.6 nm, respectively, which was in agreement with that observed from TEM image.

The unique structure formation of $Al_2O_3/Al/Al_2O_3$ composite sheet should be attributed to the electrolytic plasma and discharging on the aluminum during the PEO. In the beginning, the Al substrate was dissolved and subsequently a thin transparent passive alumina film formed on its surface. Accompanied by the alumina layer growing, the coating became more insulating, and higher voltage is demanded to produce dielectric discharge. The previous results showed that the dielectric discharge occurring through the oxide layer from the Al/Al_2O_3 interface was dominant in 15 minute with a current density of 0.04 A/cm^2 and the plasma electron temperature reached as high as 4500 ± 500 K [13]. The process is carried out in the solution at room temperature. The molten alumina was quenched immediately by the cold solution. In this case, each dielectric discharge was accompanied with the alumina melting-solidifying behavior. Thus, the formed nuclei had limited time to grow up. The produced alumina film was composed of nanosized grains.

3.2. Flexibility of the $Al_2O_3/Al/Al_2O_3$ Hybrid Composite. The bending experiments for $Al_2O_3/Al/Al_2O_3$ composite sheets as shown in Figure 2 were performed by rolling the hybrid composites on the surface of cylindrical rods with the curvature of 2 mm, 1.5 mm, and 1 mm. After bending on the 2 mm rod, there were no cracks or alumina broken appearing in the

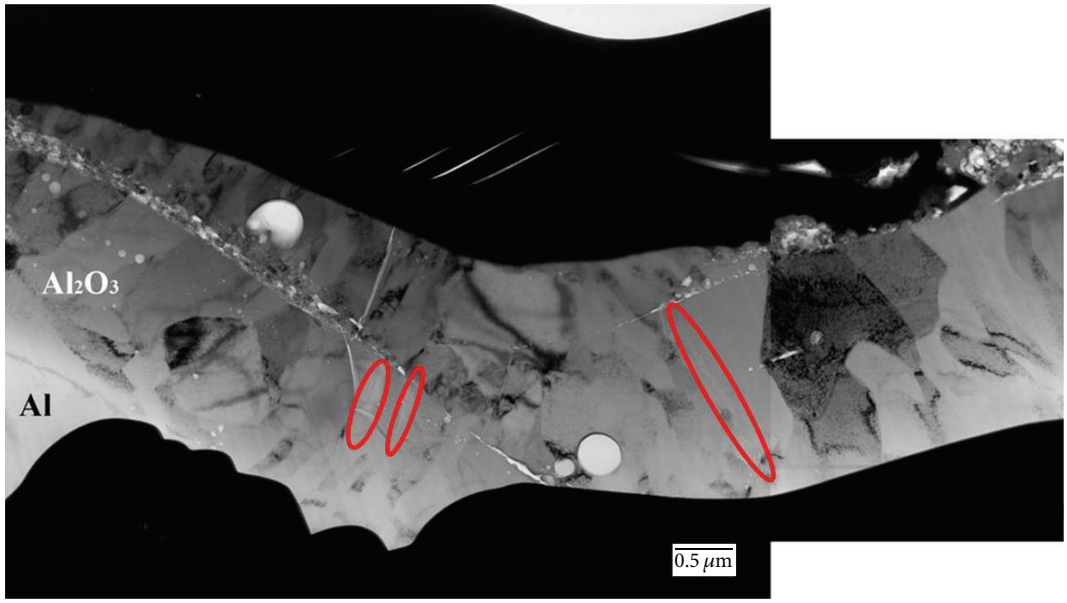

Figure 3: TEM image of the $Al_2O_3/Al/Al_2O_3$ composite sheet bent for a curvature diameter of 1.0 mm. The red ellipse labeled area shows the shear bands.

alumina layer. As the rod curvature was decreased to 1.5 mm, few cracks with a length of no more than 5 μm were observed. Further decreasing the rod curvature to 1 mm, a large number of cracks emerged in the coating along the bending axis with a zigzag shape and a length of around 30 μm. It was reported that Brazilian itacolumite, Al_2O_3-TiO_2-MgO, and $KZr_2(PO_4)_3$-$KAlSi_2O_6$ had a wonderful flexibility. However, all these ceramics are broken when the curvature exceeds 1,000 mm [4]. Evidently, the bending results indicate that the alumina in $Al_2O_3/Al/Al_2O_3$ hybrid composite possessed a flexibility and resistance against crack formation considerably higher than those of the reported flexible ceramic.

The relationship between film strain ε and diameter of curvature d is depicted in the following equation [14, 15]:

$$\varepsilon = \frac{t}{d}, \tag{1}$$

where t is the thickness of the film. For the prepared Al_2O_3 hybrid nanofilm, the thickness and bending diameter are 4.5 μm and 1.5 mm, respectively. The value of strain ε is determined to be 0.33%. Alumina ceramics are characterized by covalent and ionic bondings, and hence brittle materials at room temperature. Most of alumina ceramics are broken at strains of 0.1–0.2% or even smaller [16, 17]. It has been reported that Brazilian itacolumite, Al_2O_3-TiO_2-MgO, and $KZr_2(PO_4)_3$-$KAlSi_2O_6$ had a good flexibility. However, all these ceramics were broken with a strain no more than 0.25% [4]. Obviously, the fabricated Al_2O_3 hybrid nanofilm possesses a far higher flexibility and resistance against crack formation compared to reported flexible ceramics.

To figure out the reason why the Al_2O_3 hybrid nanofilm possesses a high flexibility, TEM analysis was employed to observe the deformation mechanisms that were active in the nanocrystalline alumina film. Firstly, the TEM image (Figure 3) shows that cracks propagated at a degree of around 60° in the film. Cracks were thought to be generated in the position of the stress fields of interfacial edge dislocations and disclination dipoles formed at interfaces (grain and interphase boundaries) during plastic deformation of nanocrystalline ceramics [18, 19]. Dislocations could initiate cracks in conventional polycrystals and nanocrystalline solids. In the Al_2O_3 nanofilm, the grain size was around 17 nm and the volume fraction of grain boundaries was remarkably greater than that in conventional coarse-grained alumina materials. Resistance of the dislocation motion was significantly enhanced. The stress needed for the commencement of plastic deformation should be somewhat high. Furthermore, the cracks in the alumina ceramic propagate in an intergranular mode [2, 20]. The propagation of nanocracks in Al_2O_3 nanofilm involved much deflection and branching which could inhibit the propagation of the cracks in turn.

Secondly, a large number of nanosized circle bubbles were distributed in the cracks area. There were two kinds of circle bubbles observed in the nanofilm. One was nanosized voids locating in the crack area, which were induced by the deformation. In particular, deformation-induced nucleation of voids occurred to release high local stresses at grain boundaries or triple junctions and ledges of grain boundaries [21]. The nanosized voids consumed energy to nucleation and forced the cracks to undergo a very tortuous path and cost a large amount of energy to pass through, which effectively hindered the propagation of the cracks. The other kind of bubbles was macrosized circle bubbles, far away from the cracks, which had size around 0.3 μm. Porosity usually plays a negative influence on the strength of the material and reduces it sharply [22]. It is worthy to note that the pores in the

Table 1: Tensile properties and coating characteristics of the Al foil and their composites.

Samples	Sample thickness (μm)	One side coating thickness (μm)	Yield strength (YS) (MPa)	Ultimate tensile strength (UTS) (MPa)	Elongation (%)	Young modulus (GPa)
Al foil	25		34.9	77.9	2.52	31.2
PEO for 4 min	25.2	1.35	73.2	91.2	2.43	59.6
PEO for 8 min	25.4	2.16	96.5	109.4	2.18	110.7
PEO for 14 min	33.1	6.86	91.4	113.8	1.15	127.4

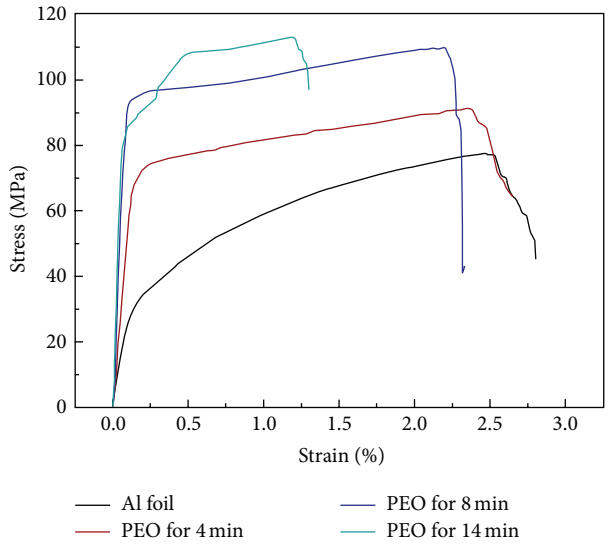

Figure 4: Engineering stress-strain curves of the $Al_2O_3/Al/Al_2O_3$ composite sheet compared to Al foil.

Al_2O_3 hybrid nanofilm prepared by PEO technique were in a circular shape, which was quite difficult to produce a stress concentration point to form a crack tip and consequently had negligible effect on the strength.

Thirdly, shear bands were formed during the bending process, as shown in the ellipse labelled area of Figure 3. The shear band type of deformation is typically observed in metallic glasses. It has also been found in some nanocrystalline materials and highlights the typical lack of ductility of nanostructured materials [23–25]. The initiation and propagation of shear bands could relieve high local stresses, resist crack formation, and enhance the flexibility of the alumina.

3.3. Tensile Properties of the $Al_2O_3/Al/Al_2O_3$ Hybrid Composite. The engineering stress-strain curves for the Al/Al_2O_3 composite sheets prepared with different PEO processing times as well as Al foil are shown in Figure 4. The mechanical properties taken from these curves are summarized in Table 1. As-received aluminum foil exhibited 77.9 MPa ultimate tensile strength (σ_{UTS}), 34.9 MPa yield strength (σ_y), and 31.2 GPa Young's modulus (E), with elongation (ε_f) of 9.6%. The addition of the nanoceramic oxides produced by the employed PEO process substantially increased the σ_{UTS}, σ_y, and E values of aluminum foil. As the thickness of nanocrystalline alumina increased to 13.72 μm (processing time being 14 min), the yield strength of the Al foil was enhanced by 162%, ultimate tensile strength raised by 45%, and Young's modulus ascended by 3.57 times. The elongation was reduced by 54%. But, with the processing time of 8 min, the elongation of the materials was only decreased by 13%. The tensile results indicate that, during tensile loading, in the elastic stage, $Al_2O_3/Al/Al_2O_3$ composite film showed a ceramic behavior of high elastic stiffness in dominance, in which nanoalumina layer played a key role. When the material entered the yield stage, the aluminum foil functioned as a load carrier.

As the PEO processing time lasting to 14 min, excessive fusion of the substrate produced the relatively thick nanoceramic coating, which led to the high yield and ultimate strengths. However, the presence of porosity in the substrate reduced elongation considerably. Also, inhomogeneous cross sections of the foil substrate due to the formation of the wavy interface between the nanocoating and the aluminum foil caused localized stress concentration, which might affect the elongation as well.

The tensile fractograph of Al foil and $Al_2O_3/Al/Al_2O_3$ composite sheets is shown in Figure 5. It can be found that the fracture of Al foil reveals a typical knife edge rupture with parallel glide steps and plastic deformation. However, as for the $Al_2O_3/Al/Al_2O_3$ composite sheet, both the rupture of the outer nanoalumina layer and ductile fracture of the inner Al foil were observed. Figure 6 shows the surface morphologies near the fracture for the Al foil and Al/Al_2O_3 composite sheet. There were lots of slip bands and slip steps distributing on the surface of Al foil. This observation might explain why the ductile Al foil underwent plastic deformation by dislocation motion. The ceramic part was split due to the lower plasticity of polycrystalline ceramic compared to Al foil, and some chipping and tortuous cracks were formed. The distances between the cracks become less as they are far away from the fracture surface. However, splitting ceramic was just like a pictured puzzle. They could be suppressed and combined together to form the morphology just as original one perpendicular to the tensile loading direction. This indicates high bonding strength present between the ceramic and Al foil. Furthermore, it can be observed that the cracks or splitting lines were along the melting columnar boundaries mentioned in Figure 1.

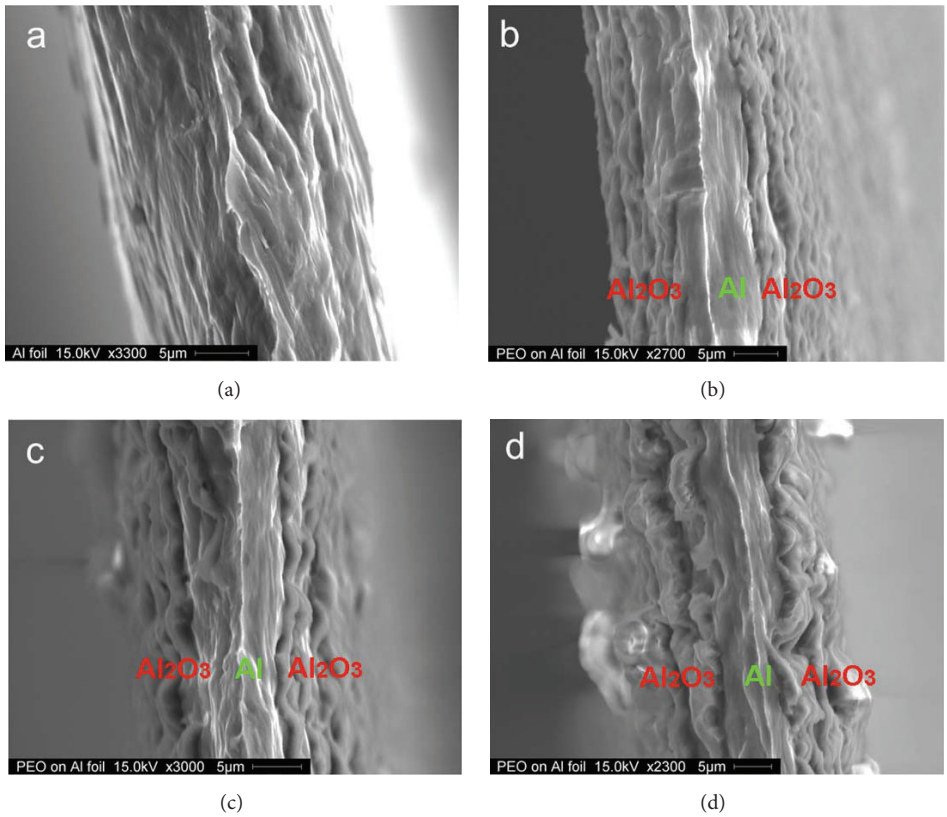

Figure 5: Tensile fracture of (a) Al foil and PEO coating for (b) 4 min, (c) 8 min, and (d) 14 min.

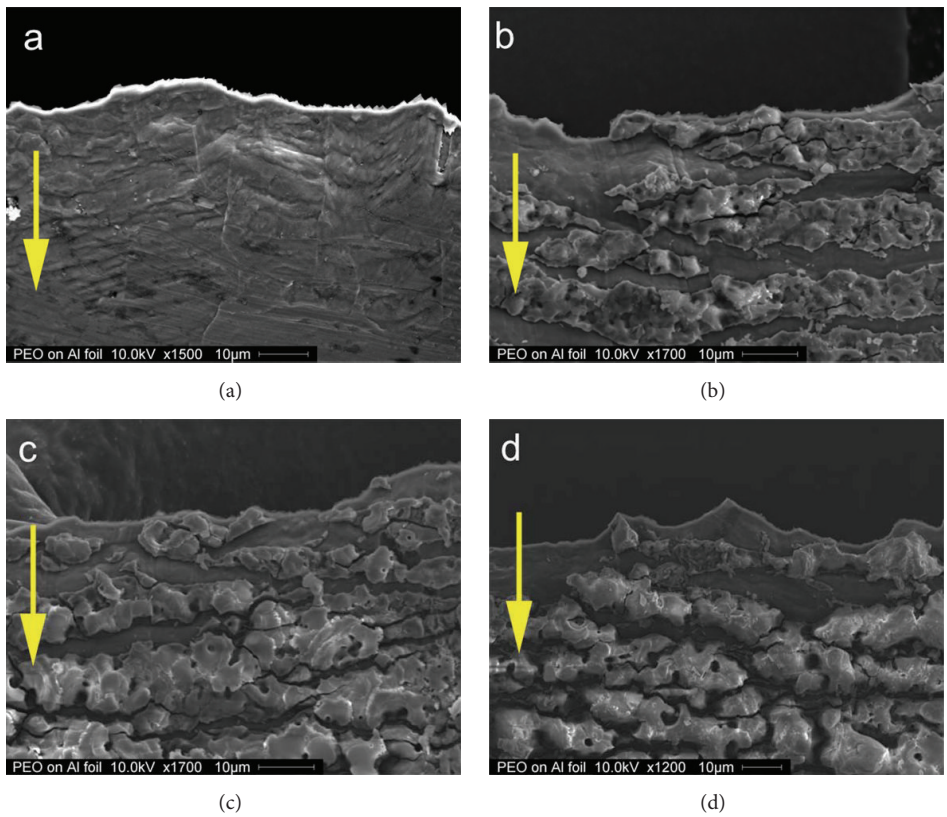

Figure 6: Surface morphology of (a) Al foil and PEO coating for (b) 4 min, (c) 8 min, and (d) 14 min. The arrow shows the tensile loading direction.

Based on the microstructure analyses and tensile results, the fracture mechanism for the $Al_2O_3/Al/Al_2O_3$ composite sheets can be proposed as follows. As the tensile loading increased in the elastic stage, deformation energy was released by forming tortuous cracks gradually in the alumina layer tightly bonded on both sides of the Al foil. When the intensity of cracking arose under high loading, the ceramic alumina reduced its role as the load bearing. The loading was shifted to the Al substrate. Once the applied stress exceeded its yield tensile strength, the $Al_2O_3/Al/Al_2O_3$ composite deformed plastically. The excellent integration of the components made the $Al_2O_3/Al/Al_2O_3$ composite exhibit both high stiffness and ductility.

4. Conclusions

By employing PEO process, flexible $Al_2O_3/Al/Al_2O_3$ hybrid composite was fabricated, of which the alumina part was composed of an inner thin compact layer and an outer columnar layer. The alumina in a polycrystalline state consisted of α-Al_2O_3 and γ-Al_2O_3 with the size of around 17 nm. The hybrid composite had a high flexibility compared to the previously reported ceramics, which should be attributed to nanocrystalline structure, shear band formation, nanosized circle bubbles prolonging the crack path, grain rotation, and deformation. When the PEO processing was applied for a desired period time, the fabricated $Al_2O_3/Al/Al_2O_3$ hybrid composite exhibited both excellent stiffness and high elongation, suggesting its great potential for practical applications.

Conflict of Interests

The authors declare that there is no conflict of interests regarding the publication of this paper.

Acknowledgments

This research was supported by the Natural Science and Engineering Research Council of Canada (NSERC) and University of Windsor.

References

[1] I.-W. Chen and X.-H. Wang, "Sintering dense nanocrystalline ceramics without final-stage grain growth," *Nature*, vol. 404, no. 6774, pp. 168–171, 2000.

[2] A. Rosenflanz, M. Frey, B. Endres, T. Anderson, E. Richards, and C. Schardt, "Bulk glasses and ultrahard nanoceramics based on alumina and rare-earth oxides," *Nature*, vol. 430, no. 7001, pp. 761–764, 2004.

[3] Y. Waku, N. Nakagawa, T. Wakamoto, H. Ohtsubo, K. Shimizu, and Y. Kohtoku, "A ductile ceramic eutectic composite with high strength at 1,873 K," *Nature*, vol. 389, no. 6646, pp. 49–52, 1997.

[4] I. Sato, Y. Ichikawa, J. Sakanoue, M. Mizutani, N. Adachi, and T. Ota, "Flexible ceramics in the system $KZr_2(PO_4)_3$-$KAlSi_2O_6$ prepared by mimicking the microstructure of itacolumite," *Journal of the American Ceramic Society*, vol. 91, no. 2, pp. 607–610, 2008.

[5] K. J. Koester, J. W. Ager III, and R. O. Ritchie, "The true toughness of human cortical bone measured with realistically short cracks," *Nature Materials*, vol. 7, no. 8, pp. 672–677, 2008.

[6] V. Imbeni, J. J. Kruzic, G. W. Marshall, S. J. Marshall, and R. O. Ritchie, "The dentin-enamel junction and the fracture of human teeth," *Nature Materials*, vol. 4, no. 3, pp. 229–232, 2005.

[7] C. Ortiz and M. C. Boyce, "Bioinspired structural materials," *Science*, vol. 319, no. 5866, pp. 1053–1054, 2008.

[8] E. Munch, M. E. Launey, D. H. Alsem, E. Saiz, A. P. Tomsia, and R. O. Ritchie, "Tough, bio-inspired hybrid materials," *Science*, vol. 322, no. 5907, pp. 1516–1520, 2008.

[9] A. L. Yerokhin, X. Nie, A. Leyland, A. Matthews, and S. J. Dowey, "Plasma electrolysis for surface engineering," *Surface & Coatings Technology*, vol. 122, no. 2-3, pp. 73–93, 1999.

[10] Z. J. Wang, X. Y. Nie, H. Hu, and R. O. Hussein, "In situ fabrication of blue ceramic coatings on wrought Al Alloy 2024 by plasma electrolytic oxidation," *Journal of Vacuum Science & Technology A: Vacuum, Surfaces and Films*, vol. 30, no. 2, Article ID 021302, 2012.

[11] U. Holzwarth and N. Gibson, "The Scherrer equation versus the 'Debye-Scherrer equation'," *Nature Nanotechnology*, vol. 6, no. 9, p. 534, 2011.

[12] H. P. Klug and L. E. Alexander, *X-Ray Diffraction Procedures*, Wiley, New York, NY, USA, 1959.

[13] R. O. Hussein, X. Nie, D. O. Northwood, A. Yerokhin, and A. Matthews, "Spectroscopic study of electrolytic plasma and discharging behaviour during the plasma electrolytic oxidation (PEO) process," *Journal of Physics D: Applied Physics*, vol. 43, no. 10, Article ID 105203, 2010.

[14] J. Rodgers, J. Edel, J. Rivera et al., "Bending of nanowire-flexible substrate assemblies integrated via direct synthesis methods," *Physica Status Solidi A—Applications and Materials Science*, vol. 208, no. 10, pp. 2443–2449, 2011.

[15] J. Lewis, "Material challenge for flexible organic devices," *Materials Today*, vol. 9, no. 4, pp. 38–45, 2006.

[16] D. J. Green, *An Introduction to the Mechanical Properties of Ceramics*, Cambridge University Press, Cambridge, UK, 1998.

[17] X. D. Han, Y. F. Zhang, K. Zheng et al., "Low-temperature in situ large strain plasticity of ceramic SiC nanowires and its atomic-scale mechanism," *Nano Letters*, vol. 7, no. 2, pp. 452–457, 2007.

[18] I. A. Ovid'ko and A. G. Sheinerman, "Nanocrack generation at dislocation-disclination configurations in nanocrystalline metals and ceramics," *Physical Review B—Condensed Matter and Materials Physics*, vol. 77, no. 5, Article ID 054109, 2008.

[19] W.-F. Rao and Y. U. Wang, "Domain wall broadening mechanism for domain size effect of enhanced piezoelectricity in crystallographically engineered ferroelectric single crystals," *Applied Physics Letters*, vol. 90, no. 4, Article ID 041915, 2007.

[20] H. Gleiter, "Nanostructured materials: basic concepts and microstructure," *Acta Materialia*, vol. 48, no. 1, pp. 1–29, 2000.

[21] I. A. Ovid'Ko, A. G. Sheinerman, and N. V. Skiba, "Elongated nanoscale voids at deformed special grain boundary structures in nanocrystalline materials," *Acta Materialia*, vol. 59, no. 2, pp. 678–685, 2011.

[22] L. Wu, Y. D. Huang, Z. J. Wang, and L. Liu, "Controlled fabrication of porous Al_2O_3 ceramic by N,N′-dimethylformamide-based gel-casting," *Scripta Materialia*, vol. 62, no. 8, pp. 602–605, 2010.

[23] M. D. Demetriou, M. E. Launey, G. Garrett et al., "A damage-tolerant glass," *Nature Materials*, vol. 10, no. 2, pp. 123–128, 2011.

[24] B. J. Dalgleish and A. G. Evans, "Influence of shear bands on creep rupture in ceramics," *Journal of the American Ceramic Society*, vol. 68, no. 1, pp. 44–48, 1985.

[25] H. Guo, P. F. Yan, Y. B. Wang et al., "Tensile ductility and necking of metallic glass," *Nature Materials*, vol. 6, no. 10, pp. 735–739, 2007.